EDGE ARTICLE

Check for updates

Skeletal diversity in Pt- and Au-catalyzed annulations of allenedienes: dissecting unconventional mechanistic pathways†

Ronald Nelson, [ID] ‡[ab] Martín Calvelo, [ID] ‡[a] Rebeca García-Fandiño, [ID] [a] Agustí Lledós, [ID] [c] Gregori Ujaque,[c] José L. Mascareñas [ID] *[a] and Fernando López [ID] *[ad]

We describe the discovery of unprecedented annulation processes of 1,7-allenedienes, promoted by Pt or Au catalysts. These transformations revealed mechanistic pathways that had not been previously observed in reactions involving carbophilic catalysis. In particular, we have found that allenedienes bearing a silyl ether in the carbon tether connecting the diene and the allene divergently afford cyclopropane-embedded tricyclic derivatives, 6,6-fused bicarbocyclic products or 5,6-fused bicarbocyclic systems, depending on the type of Au or Pt catalyst used. We have carried out experimental and computational studies that shed light on the mechanistic reasons behind this rich and unusual skeletal divergence, and provide new lessons on the drastic influence of platinum ancillary ligands on the reaction outcome.

Introduction

Throughout the last two decades, carbophilic catalysis has reshaped the field of organic synthesis by providing an extensive portfolio of methods that allow transformation of simple unsaturated precursors into highly valuable cyclic skeletons.[1]

Our group has contributed to this field with the development of a variety of Pt- and Au-catalyzed formal cycloadditions involving allenes as key reaction partners.[2,3] In particular, in 2009, we and the Toste group, independently demonstrated that gold(I) complexes of type LAuCl/AgX could efficiently promote intramolecular cycloadditions of allenedienes of type **1** in a reagent-controlled, divergent manner (Scheme 1a).[4–6] Thus, while gold catalysts bearing σ-donating ligands such as IPr (**Au1**) or JohnPhos (**Au2**) lead to 5,7-fused bicyclic systems **2** (or

a Centro Singular de Investigación en Química Biolóxica e Materiais Moleculares (CiQUS), Departamento de Química Orgánica, Universidade de Santiago de Compostela, 15782 Santiago de Compostela, Spain. E-mail: joseluis.mascarenas@usc.es
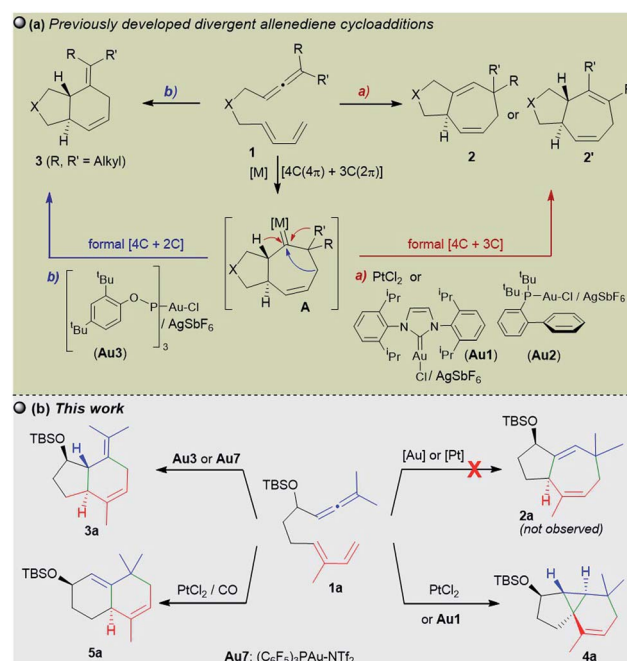
b Departamento de Química, Universidad Católica del Norte, Av. Angamos 0610, Antofagasta, Chile

c Departament de Química, Universitat Autònoma de Barcelona, Cerdanyola del Valles, 08193, Catalonia, Spain

d Instituto de Química Orgánica General CSIC, Juan de la Cierva 3, 28006, Madrid, Spain. E-mail: fernando.lopez@csic.es

† Electronic supplementary information (ESI) available: Full experimental procedures, optimization of the catalyst, characterization of all new compounds (including NMR spectra), computational details (including Fig. S8–S18), and Cartesian coordinates are provided. CCDC 1964184–1964188. For ESI and crystallographic data in CIF or other electronic format see DOI: 10.1039/d0sc00650e

‡ R. N. and M. C. contributed equally.

2′), through a formal [4C + 3C] cycloaddition (Scheme 1a, a), catalysts featuring bulky π–acceptor ligands such as **Au3** afford [4C + 2C] adducts (**3**), provided that terminally disubstituted allenes are used (Scheme 1a, b). Theoretical and experimental data confirmed that the reactions involve a common metal

Scheme 1 (a) Previous Au(I) and Pt(II)-catalyzed allenediene cycloadditions and (b) current divergent annulations.

carbene intermediate (**A**), which evolves from 1,2-hydride or 1,2-alkyl migrations to deliver the observed adducts. The divergence of the process is controlled by stereoelectronic factors of the ancillary ligand, the cationic character of the gold carbene, and the substitution pattern at the carbene adjacent positions.[4b,7] Therefore, in several cases, mixtures of cycloheptene (**2/2′**) and cyclohexene (**3**) adducts are obtained.

Remarkably, the performance of the Au(I) catalysts contrasts with that of their Pt(II) counterparts which, albeit less active, had been previously shown to deliver exclusively cycloheptene products (**2/2′**).[8,9] Indeed, we have exploited this selectivity in short total synthesis of Englerin A, a sesquiterpene natural product with antitumor properties.[10]

The catalyst-dependent [4C + 3C]/[4C + 2C] annulation of allenedienes was further confirmed by other groups,[5,11] and thus it seemed to be a well-established reactivity paradigm. However, we have now found new, surprising annulation pathways that revealed unprecedented ligand-dependent skeletal rearrangements. In particular, we demonstrate herein that 1,7-allenedienes with a silyl ether pendant in the tether (*e.g.* **1a**) can divergently afford cyclopropane-embedded tricyclic derivates of type **4**, 6,6-fused bicarbocyclic products such as **5**, or 5,6-fused bicyclic adducts **3**, depending on the Au or Pt catalyst employed (Scheme 1b). The drastic reactivity switch when the PtCl$_2$-catalyzed reactions are carried out in the presence of CO, an effect that is absent in previous Pt-catalysed reactions, is particularly relevant. Curiously, we did not observe the otherwise expected [4 + 3] adducts of type **2** (**2a/2a′** Scheme 1b).

More importantly, we describe mechanistic studies that shed light on the reasons behind this divergence, and reveal unanticipated pathways that had never been observed in carbophilic metal catalysis. Thus, our work confirms the importance of generally overlooked homo-hyperconjugative interactions in Pt catalysis and shows how subtle conformational and stereoelectronic factors can critically determine the reaction outcome.

Results and discussion

Initial results: discovery of catalyst-dependent multifold paths of allenedienes

We initiated our studies by analyzing the cycloaddition of allenediene **1a**, which was designed as a potential precursor of the carbocyclic core of guaiane sesquiterpenes.[12] Surprisingly, when allenediene **1a** was treated with IPrAuCl/AgSbF$_6$ (**Au1**) in CH$_2$Cl$_2$, the adduct **2a** was not observed. Instead, we obtained a 1 : 2 mixture of the formal [4C + 2C] adduct **3a** and the cyclopropyl derivative **4a** (isolated in 57% yield), which
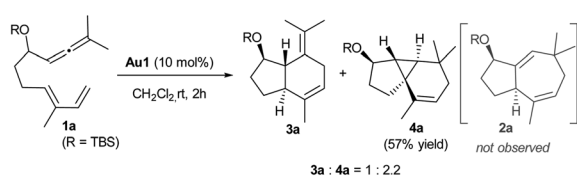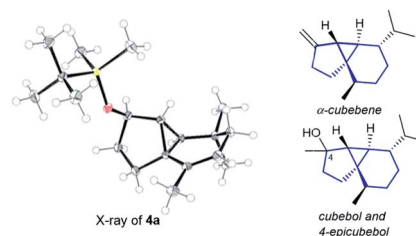

Fig. 1 X-ray structure of **4a**,[13] and the sesquiterpenes cubebols and a cubebene.

exhibited an unanticipated 5,3,6-tricyclic skeleton with four consecutive stereocenters (Scheme 2).

The structure and relative stereochemistry of both products were determined by NMR, and those of **4a** were confirmed by X-ray analysis (Fig. 1).[13] This type of tryciclo[4.4.0.0^{1,5}]decane skeleton is relevant as it forms the basic core of important natural products like cubebenes, currently used in the fragrance and food industries.[14] Notably, while previous routes to these scaffolds involve numerous steps from chiral pool sources,[15] the above annulation proposes a straightforward, fully stereoselective entry to their basic cores from readily accessible acyclic precursors.[16]
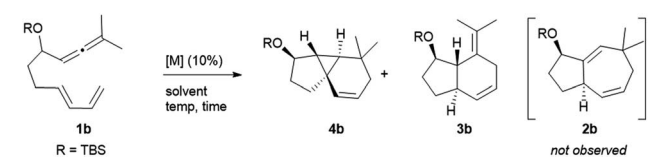
The synthetic relevance of the tricyclic product and, specially, the intriguing mechanistic features of the transformation, prompted us to further study the process. The reaction promoted by **Au1** can be reproduced in substrate **1b**, an allenediene that lacks the methyl group in the diene (Table 1). Again, we obtained a mixture of the tricyclic product **4b** and the formal [4C + 2C] adduct **3b**, with good selectivity towards the former (**4b** : **3b** = 5 : 1). Accordingly, the cyclopropyl adduct **4b** was isolated in a good 70% yield.

Interestingly, other gold(I) complexes previously reported to promote formal [4C + 3C] cycloadditions of allenedienes, also failed to give the cycloheptenyl adduct **2b**. Thus, while the JohnPhos-based catalyst **Au2′** provided a complex mixture of products (entry 2), gold(I) complexes with Xphos and Ruphos ligands provided very modest yields of **4b** (entries 3 and 4). Noteworthily, the *N*-heterocyclic carbene gold complex IPr^{Me}AuCl/AgNTf$_2$ (**Au6**) was completely selective towards the tricyclic product **4b** (96% yield at rt, entry 5).

In consonance with previous reports, the formal [4C + 2C] adduct **3b** could be obtained in good yields when complexes bearing π–acceptor ligands, such as **Au3** or **Au7**, are used as catalysts (entries 6–7).[4b,5] On the other hand, gold(III) complexes such as AuCl$_3$ or AuBr$_3$ provided complex mixtures at rt (entries 8 and 9), whereas the 2-picolinate derivative PicAuCl$_2$ showed some reactivity at high temperature (refluxing toluene), but gave a very modest yield of **4b** (17%, after 8 h, entry 10).

Surprisingly, the reaction of **1b** with catalytic amounts of PtCl$_2$, in refluxing toluene, also provided the tricyclic product **4b** with complete selectivity, but with moderate yield (entry 11). Other catalysts such as [PtCl$_2$(ethene)$_2$]$_2$ or PtCl$_2$/P(C$_6$F$_5$)$_3$ afforded the same product in moderate to good yields, under otherwise identical reaction conditions (entries 12–13). Amongst these catalysts, PtCl$_2$ turned out to be the most

Scheme 2 Unexpected reaction outcome of **1a** using IPrAuCl/AgSbF$_6$ (**Au1**).

Table 1 Exploration of the cycloaddition of **1b**; selectivity with different Au and Pt catalysts[a]

| Entry	[M]	T (°C)	t (h)	**4b** : **3b** ratio[b]	Yield[c] (%)
1	IPrAuCl/AgSbF$_6$ (**Au1**)	rt	2	5 : 1	70 (**4b**)
2	JohnPhosAuNTf$_2$ (**Au2'**)	rt	12	—	—[d]
3	XPhosAuNTf$_2$ (**Au4**)[e]	80	12	1.1 : 1	18 (**4b**)
4	RuPhosAuNTf$_2$ (**Au5**)	40	12	16 : 1	32 (**4b**)
5	IPr^{Me}AuCl/AgNTf$_2$ (**Au6**)	rt	2	1 : 0	96 (**4b**)
6	(ArO)$_3$PAuCl/AgSbF$_6$ (**Au3**)[f]	−15	1.5	1 : 7	66 (**3b**)
7	(C$_6$F$_5$)$_3$PAuCl/AgNTf$_2$ (**Au7**)[g]	−15	1	1 : 12	70 (**3b**)
8	AuCl$_3$	rt	12	—	—[d]
9	AuBr$_3$	rt	12	—	—[d]
10[h]	PicAuCl$_2$	110	8	1 : 0	17 (**4b**)
11[h]	PtCl$_2$	110	0.5	1 : 0	43 (**4b**)
12[h]	[PtCl$_2$(ethene)$_2$]$_2$[g]	110	1	1 : 0	53 (**4b**)
13[h]	PtCl$_2$/(C$_6$F$_5$)$_3$P (1 : 1)	110	1	1 : 0	62 (**4b**)
14[h]	PtCl$_2$	70	2	1 : 0	81 (**4b**)
15[i]	PtCl$_2$	50	2	1 : 0	88 (**4b**)
16[j]	PtCl$_2$	30	2.5	1 : 0	99 (**4b**)
17[j]	PtCl$_2$ (1 mol%)	30	24	1 : 0	92 (**4b**)

[a] Carried out with [M] (10 mol%) in CH$_2$Cl$_2$ (0.05 M), unless otherwise noted. See Tables S1–S2 for the structures of Au complexes and further examples. [b] Ratio determined by ^{1}H-NMR of the crude mixtures. [c] Isolated yield. [d] Complex mixture of products. [e] Carried out in 1,2-DCE. [f] Ar = 3,5-(^{t}Bu)$_2$C$_6$H$_3$. [g] Carried out with 5 mol% catalyst. [h] Carried out in toluene. [i] Carried out in cyclohexane (with 1 ppm of water). [j] Carried out in 1,4-dioxane.

efficient one, providing a 81% yield at 70 °C (entry 14). The solvent also played a key role in the rate and efficiency of the process: cyclohexane and 1,4-dioxane proved to be optimal, respectively delivering **4b** in 88% yield (2 h at 50 °C, entry 15) and 99% yield (2.5 h at 30 °C, entry 16). Moreover, the reaction could be scaled up (gram scale), and the amount of the catalyst could also be reduced to 1 mol%, without notably affecting the yield and/or selectivity (entry 17).

Surprisingly, when the reaction of **1b** with PtCl$_2$ was carried out in the presence of CO (balloon) – a strategy that has been previously employed to accelerate PtCl$_2$ catalyzed processes – we observed a new type of adduct, the biscyclohexenyl product **5b** (59% yield), together with minor amounts of **4b** (**5b** : **4b** ratio = 8 : 1, Scheme 3). X-ray analysis of a desilylated derivative (**5b'**) confirmed its 6,6-bicyclic structure.[13]

This type of bicarbocyclic skeleton is quite common in several sesquiterpenes (Scheme 3, bottom).[17] Importantly, carrying out the reaction in cyclohexane (with a 1 ppm content of water) at 50 °C for 2 h resulted in **5b** in 85% yield (**5b** : **4b** ratio = 9 : 1). While using completely dry cyclohexane the reaction was slightly less efficient (79% yield, Scheme 3; also see Table S3†).
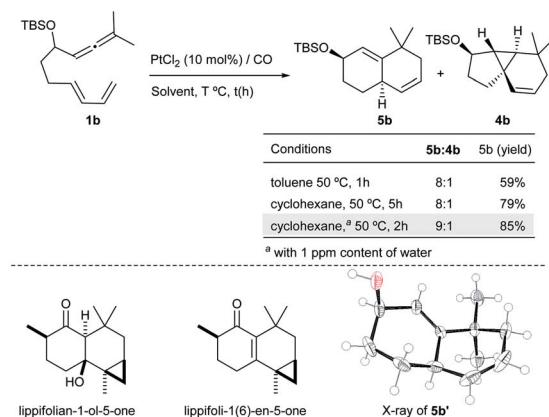
Scheme 3 PtCl$_2$-catalyzed reaction of **1b** under a CO atmosphere.
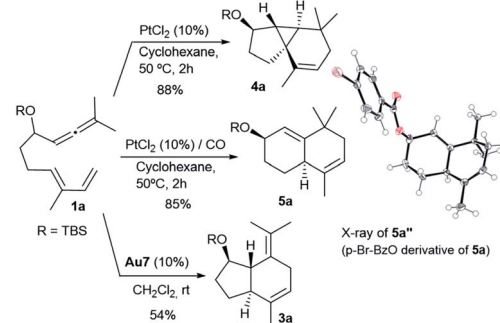
Scheme 4 Catalyst-dependent skeletal diversity from **1a**.

Chemical Science

In analogy with the above results, treatment of the precursor **1a** with PtCl$_2$, in cyclohexane at 50 °C, gave the tricyclic adduct **4a** (88% yield), whereas performing this reaction under a CO atmosphere produced the bicarbocyclic adduct **5a** in 85% yield (Scheme 4). Alternatively, when using **Au7** as the catalyst, the same precursor (**1a**) provides the expected 5,7-fused bicyclic product **3a** (54% yield, formal [4 + 2] cycloadduct).[13]
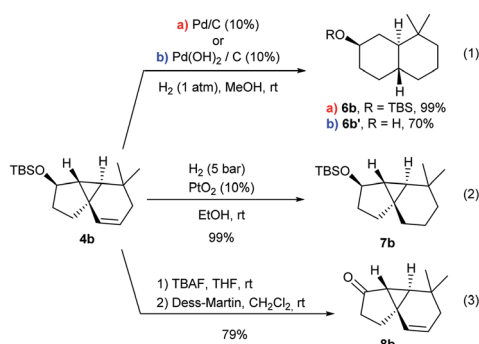
Overall, these results confirm an interesting case of multi-fold reactivity, in which the acyclic precursor can be transformed in a catalyst-dependent, divergent manner. Moreover, the above-described examples represent the first demonstration of a drastic change in the outcome of a Pt-catalyzed reaction, when it is carried out in the presence of CO.[18]

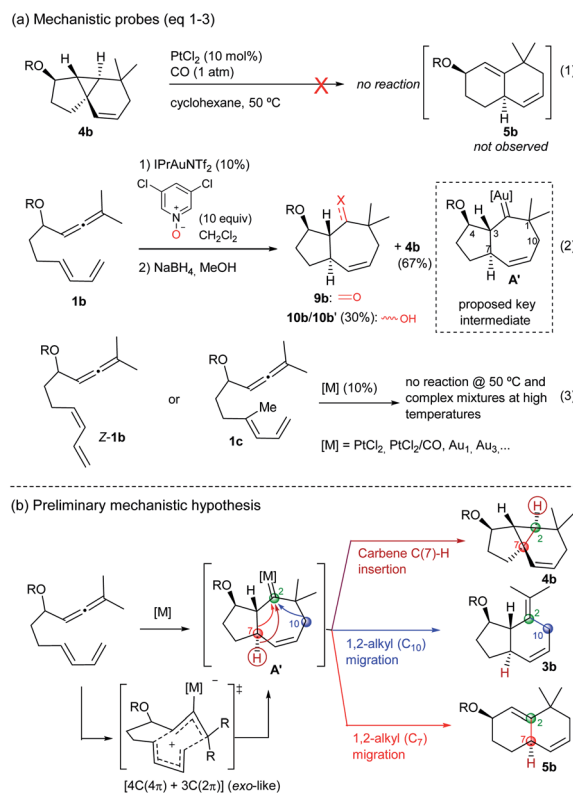## Preliminary exploration of the synthetic potential of the products

A preliminary analysis of the synthetic potential of the tricyclic adducts **4** revealed interesting reactivity profiles (Scheme 5). Therefore, treatment of **4b** with H$_2$ (1 atm) over Pd/C (10 mol%) resulted in the hydrogenation of the double bond with concomitant cyclopropane opening, affording the *trans*-fused bicyclic product **6b** in quantitative yield and with complete diastereoselectivity (Scheme 5, eqn (1), conditions *a*).[19] An alternative hydrogenation using Pd(OH)$_2$/C in MeOH also proceeded with equal selectivity, albeit the TBS group was also removed (eqn (1), conditions *b*). In contrast, the use of PtO$_2$ (10 mol%) under H$_2$ pressure (5 bar) led to the exclusive hydrogenation of the double bond, quantitatively affording the tricyclic system **7b**, which presents a carbocyclic core analogous to that of cubeb derivatives (eqn (2)). Finally, the OTBS group of **4b** could also be easily converted into its corresponding ketone (**8b**), paving the way for further variations at this position (eqn (3)).

Experimental mechanistic studies

The above annulation reactions are especially intriguing from a mechanistic perspective. In this context, we first questioned whether the 6,6-bicarbocyclic cycloadducts (such as **5b**) could be formed by cleavage of the cyclopropyl ring in the adduct **4b**. However, treatment of this tricyclic compound with PtCl$_2$/CO, under standard conditions, neither generated **5b** nor any other


Scheme 6 (a) Mechanistic probes (eqn (1)–(3)) and the (b) mechanistic hypothesis.

identifiable product (Scheme 6a, eqn (1) and Tables S4–S6†).[13] Given that the mechanistic proposals to explain the formation of adducts **2** and **3** invoked the presence of carbene intermediates (**A**, Scheme 1), and envisioning that the same type of intermediate could also be behind the novel reactivity, we sought to trap the putative carbene species using different oxidants.[20] Gratifyingly, after some experimentation (Table S7†), we found that treatment of **1b** with IPrAuNTf$_2$ (10 mol%) and 3,5-dichloropyridine oxide (10 equiv) provided, together with the tricyclic adduct **4b** (67% yield), a substantial amount of the ketone **9b** ($\approx$30% yield, Scheme 6, eqn (2)). This product was identified after reduction of the crude residue with NaBH$_4$, which afforded the alcohols **10b** and **10b'** (30% overall yield). Although this result is not fully conclusive, as the pyridine oxide

Scheme 5 Preliminary exploration of the synthetic potential of adducts 4.
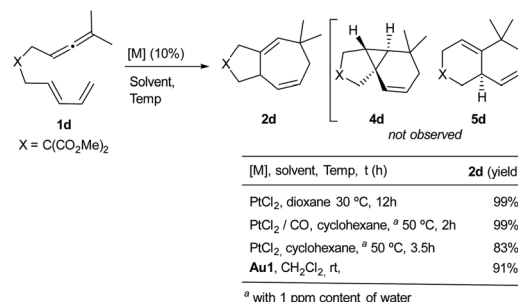
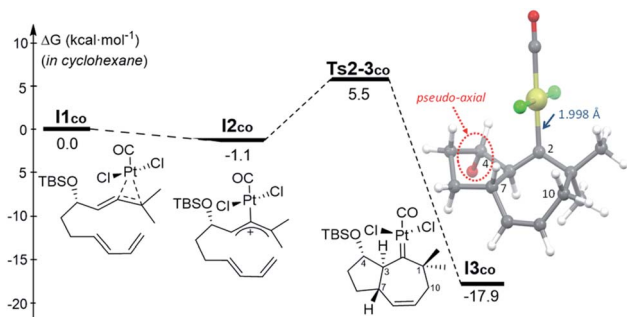Scheme 7 Pt(II)- and Au(I)-catalyzed annulations of 1d.

Fig. 2 Gibbs energy profile (kcal mol^{-1}) for the activation of **1b** by PtCl$_2$(CO) and its subsequent [4C + 3C] cycloaddition in cyclohexane (SMD model). The TBS group is omitted from the 3D representation of **I3$_{co}$** for clarity.[22]

could somehow alter the mechanistic pathway, the formation of cycloheptenone **9b** is *a priori* compatible with a concerted allenediene [4C(4π) + 3C(2π)] cycloaddition that delivers the hypothesized carbene species **A′** (Scheme 6a, eqn (2)).

Importantly, allenedienes **Z-1b** and **1c**, respectively bearing a *cis*-conjugated diene or a methyl group at the diene internal position, did not provide any product regardless of the type of the catalyst used (Scheme 6a, eqn (3), Tables S8–S9†). These results are consonant with a concerted cycloaddition to provide a metal carbene species like **A′** (Scheme 6b), which can evolve in a divergent way to give the observed products. Indeed, we initially envisioned that a putative C(7)–H carbene insertion could provide the tricyclic adduct of type **4**,[21] whereas alternative 1,2-alkyl migrations of C10 and C7, with concomitant

elimination of the catalyst, would produce the adducts **3** (migration of C10) and **5** (migration of C7) (Scheme 6b).

Other allenediene precursors with OTIPS or OTES groups in the tether also provided the same reactivity profile as **1a** or **1b** (Table S10†). However, treatment of allenediene **1d**, equipped with a gem-diester in the tether, with PtCl$_2$ produced the expected seven-membered cycloadduct **2d** in quantitative yield (Scheme 7).[8] Moreover, when this reaction was carried out under a CO atmosphere, in cyclohexane, we observed the same product (**2d**) again. Likewise, we also obtained the adduct **2d** by using the gold catalyst **Au1**. Neither the 6,6-fused bicyclic adduct **5d** nor the tricyclic product **4d** was detected. These results confirm that the structure of the precursor also has a critical influence on the reaction outcome.

DFT analysis of the new, divergent processes

The observation that, even in the presence of CO, **1d** performs very differently from **1a** and **1b**, added further interest to the mechanistic study, and to uncover the reasons behind the skeletal divergence. We therefore performed extensive DFT computational studies, using allenedienes **1b** and **1d**, and different Pt and Au complexes as catalysts.[22]

Reaction profile for 1b using [PtCl$_2$(CO)] as the catalyst.[23] The Gibbs energy profile for the reaction of **1b** promoted by PtCl$_2$(CO) is shown in Fig. 2 and 3, together with the most relevant stationary points (see also Fig. S8–S9†). After initial coordination of the allene moiety to PtCl$_2$(CO) (**I1$_{co}$**) and generation of the Pt-substituted allyl cation **I2$_{co}$**, there is a concerted *exo*-like [4C(4π) + 3C(2π)] cycloaddition, with an energy barrier of only 6.6 kcal mol^{-1} (*via* **Ts2-3$_{co}$**). In this
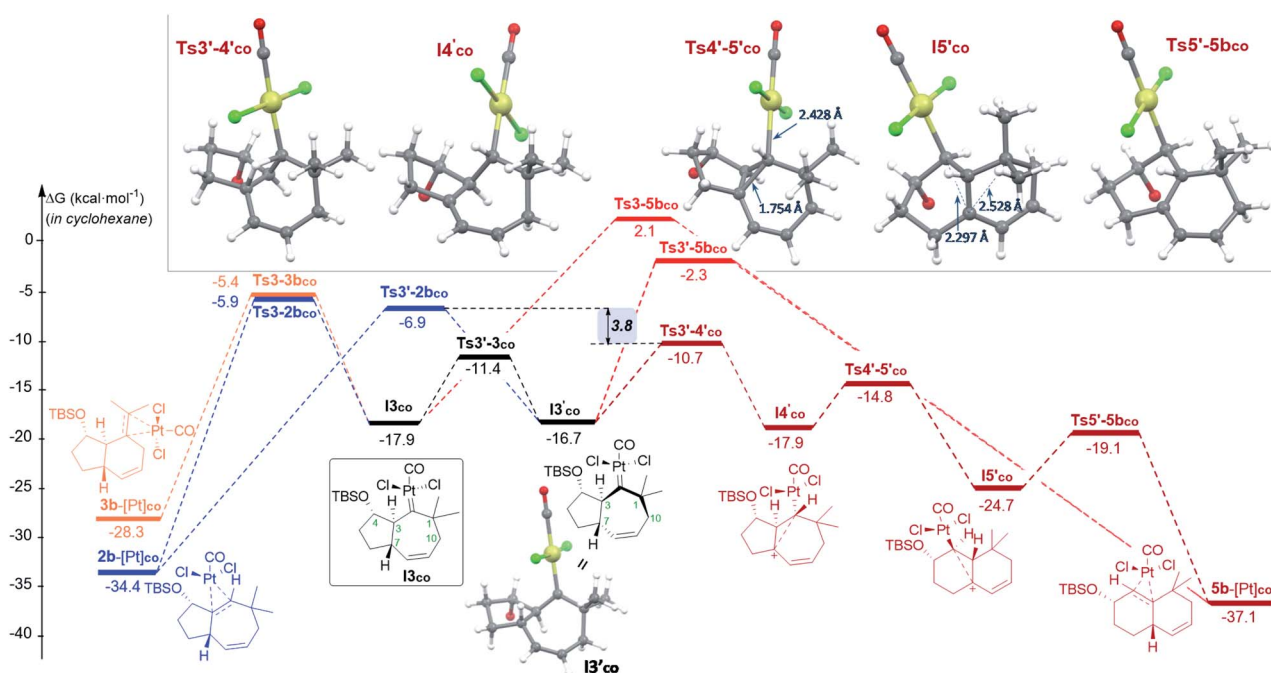

Fig. 3 Gibbs energy profile (kcal mol^{-1}) of the reaction of **1b** with PtCl$_2$(CO) in cyclohexane: the most relevant divergent pathways from **I3$_{co}$** (energy of **I1$_{co}$**, shown in Fig. 2, is considered as the reference; see Fig. S8–S9† for a complete profile).[22] Optimized structures of selected stationary points (TBS omitted for clarity).

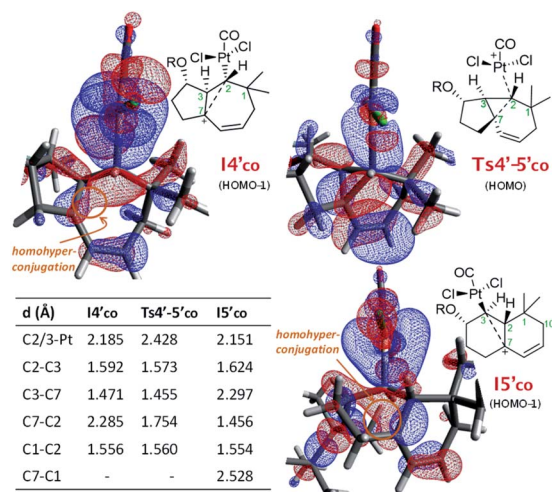| d (Å)	I4'co	Ts4'-5'co	I5'co
C2/3-Pt	2.185	2.428	2.151
C2-C3	1.592	1.573	1.624
C3-C7	1.471	1.455	2.297
C7-C2	2.285	1.754	1.456
C1-C2	1.556	1.560	1.554
C7-C1	-	-	2.528

Fig. 4 Key distances and NBO representation of relevant HOMO's of I4'co, Ts4'-5'co and I5'co. The TBS groups are truncated for clarity.[22]

cycloaddition, the OTBS group prefers to be placed in a *pseudo*-axial disposition, affording the 5,7-bicyclic carbene intermediate I3co, which is also thermodynamically favored over the *pseudo*-equatorial conformer (I3co^eq) by 3.0 kcal mol⁻¹ (Fig. S9†).[24]

From the cycloheptenyl carbene I3co, we could locate a transition state for the 1,2-alkyl migration of carbon C7 (seven-membered ring contraction, Ts3-5bco), which generates the experimentally observed dicyclohexene product 5b (denoted as 5b-[Pt]co, Fig. 3, red path, E_a: 20 kcal mol⁻¹). However, the 1,2-alkyl (C10) migration leading to the formal [4 + 2] adduct 3b (denoted as 3b-[Pt]co), and the 1,2-hydrogen (H-3) migration leading to cycloheptene 2b (denoted as 2b-[Pt]co) were found to involve significantly lower energy barriers (Fig. 3, blue and orange paths).

Importantly, more detailed DFT scrutiny revealed an unanticipated but energetically more viable alternative, which is initiated by a conformational change in Pt–carbene species I3co to generate I3'co, a conformer in which five out of the seven carbons of the cycloheptene (C3, C7–C10) are almost coplanar (Fig. 3). This species is 1.2 kcal mol⁻¹ less stable than I3co, but accessible through an activation barrier of only 6.5 kcal mol⁻¹ (see Fig. 3 and S8†). Therefore, this easy conformational evolution warrants eventual Curtin–Hammet conditions.

From I3'co we located an unexpected, very favorable migration of the hydrogen at C7 to the Pt–carbene center (C2) to give the carbocationic intermediate I4'co (Fig. 3, magenta path). This is an interesting species which can be viewed as a non-classical carbocation stabilized by homohyperconjugation (also called the γ-effect),[25] namely donation of electron density from the back lobe of the Pt–C2 orbital to the empty p orbital of C7. The HOMO−1 molecular orbital of I4'co, obtained by NBO analysis, clearly shows that it is the hyperconjugation, rather than a hypothetical allyl-cation conjugation (with the C8–C9 double bond), what accounts for the relative stability of I4'co (Fig. 4).[26]

The atoms in molecules (AIM) topological analysis of I4'co further confirms this bonding pattern, providing for C2 a sum

of Wiberg bond indexes (WBIs) of 3.91, a value which is divided into five different bonds. Thus, this analysis provided WBIs of 0.18 and 0.52 for the critical C2–C7 and C2–Pt bonds, whereas those of C2–C3 and C3–C7 bonds are clearly higher, 0.89 and 1.07, respectively (Fig. S10†).[27]

Importantly, the evolution of I3'co to I4'co is much more favorable than either the 1,2-hydride migration towards 2b (via Ts3'-2bco), or the 1,2-alkyl (C7) migration via Ts3'-5bco [ΔΔG‡ = 3.8 and 8.4 kcal mol⁻¹, respectively; Fig. 3].[28]

Curiously, DFT calculations indicate that intermediate I4'co could undergo a very easy skeletal rearrangement to the more stable 6,6-bicyclic system I5'co, through an early transition state (Ts4'-5'co, ΔG = 3.1 kcal mol⁻¹), which shows how the C2–C7 bond is being formed with net inversion of configuration at C2 [d(C2–C7) = 1.754 Å] while the Pt complex migrates stereospecifically from C2 to C3. The three different C–C bonds of the cyclopropyl ring generated in this transition state are mostly, but not completely formed (see Fig. 4 for C–C bond distances, and Fig. S10† for WBIs and Laplacian electron density maps). Also, remarkably, in this transition state, the Pt, C2, C3 and C7 atoms, together with the p orbital of C7, adopt a W-shape conformation similar to that found in cyclopropanation reactions of different organometallic species (e.g. Fe, Sn,…), wherein hyperconjugative interactions are also critical.[29]

The higher stability of I5'co compared to I4'co (6.8 kcal mol⁻¹) is probably the consequence of the release of ring strain and the strengthening of homohyperconjugative interactions. Indeed, the HOMO−1 molecular orbital of I5'co (NBO analysis) shows clear homo-hyperconjugative stabilization by an orbital that extends over C3 and C7 (Fig. 4). Accordingly, the C7–C3 distance in I5'co (2.297 Å) is significantly shorter than that of the C7–C1 bond (2.528 Å, Fig. 3 and 4). Finally, from I5'co, a stereospecific 1,2-migration of the hydrogen at C3 to the carbocation center (C7), with concomitant elimination of PtCl₂(CO), delivers the experimentally observed product 5b, which is complexed to the Pt center (denoted as 5b-[Pt]co).

Overall, the above-calculated route towards 5b from I3'co is highly exergonic and proceeds through transition states that exhibit the lowest energy barriers of all the different calculated profiles (ΔG‡ varying from 3.1 to 6.0 kcal mol⁻¹; Fig. 3). Therefore, these data are fully consistent with the experimental observation of adduct 5b as the major product in the reactions promoted by PtCl₂ under a CO atmosphere.[30]

Reaction profile for 1b using PtCl₂(ethene) as the catalyst. We next analyzed the energy profile with a Pt catalyst that affords the cyclopropyl-containing tricyclic product 4. In particular, we focused on PtCl₂(ethene)₂ since it provides the same selectivity as PtCl₂ (see Table 1, entry 12), but its four coordinating sites at the square planar Pt centre are well defined, providing an accurate model for computational studies.[31]

The overall profile for this Pt catalyst is similar to that previously found for PtCl₂(CO), but with some key differences (Fig. 5 and S12†). As in the previous case, we found that the conformational change from I3et to I3'et is instrumental in revealing the most favorable energy alternatives (for a complete profile including less favored pathways from I3et, see Fig. S12†).
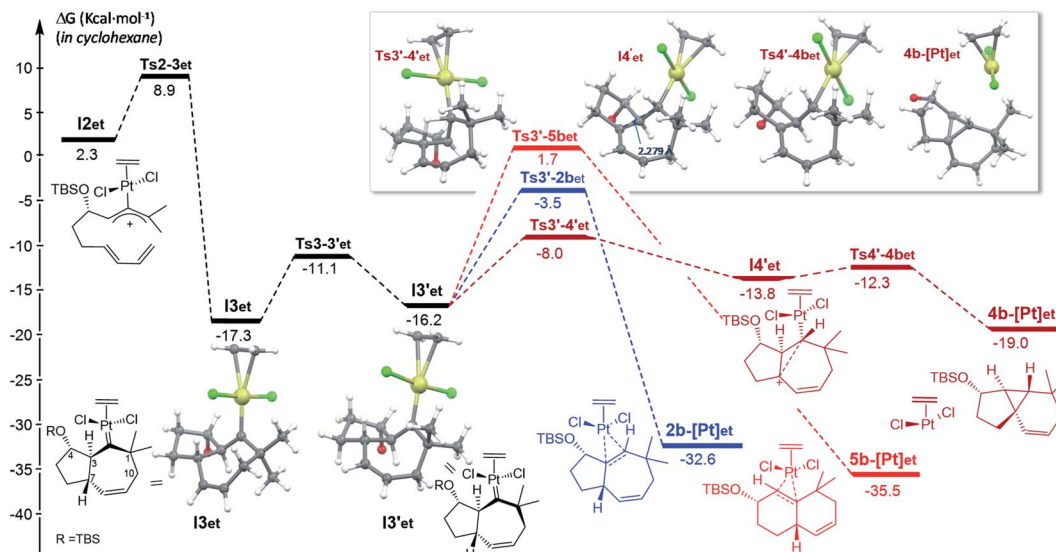
Fig. 5 Gibbs energy profile (kcal mol^{-1}) for the reaction of **1b** catalyzed by PtCl$_2$(ethene) in cyclohexane; energy of **I1$_{et}$** (Fig. S12,† complete profile) is considered as the reference.[22] Optimized structures of selected stationary points (TBS omitted for clarity).

For **I3′$_{et}$**, the lowest energy barrier of the processes involves a 1,3-hydrogen migration from C7 to the carbene center (C2), to deliver the carbocationic species **I4′$_{et}$** ($\Delta G^{\ddagger} = 8.2$ kcal mol^{-1}), also stabilized by homohyperconjugation.

Importantly, the presence of ethene at the platinum center, instead of CO, determines a different evolution of this intermediate (*vs.* **I4′$_{co}$**). Indeed, it undergoes a very easy transformation (*via* **Ts4′-4b$_{et}$**, $\Delta G^{\ddagger} = 1.5$ kcal mol^{-1}) into the cyclopropyl-containing product **4b**, with the Pt complex [PtCl$_2$(ethene)] completely de-coordinated from cyclopropane. Overall, the transformation from **I3′$_{co}$** into the cyclopropane **4** constitutes a stepwise C(sp^3)–H insertion on a Pt-carbene with concomitant cyclopropanation. This is a very uncommon pathway that, to the best of our knowledge, is unprecedented for Pt–carbene species.[32]

Therefore, the carbocationic species **I4′** evolves differently depending on whether the platinum contains a CO ligand or not. The reasons behind this ligand-dependent dichotomy are

not fully clear, but they are likely related to the particularly strong σ-donor properties of the CO ligand. Some insights could be obtained from the NBO analysis, which indicates that the carbon attached to the Pt center (C2), has a higher negative charge in **I4′$_{co}$** than in **I4′$_{et}$**.[33] This might favor stronger homo-hyperconjugation interactions in the former, hampering the decoordination of the Pt–CO complex while favoring the rearrangement and migration of the metal from C2 to C3. Moreover, the Pt atom has a more cationic character in Pt–ethene complexes than in their analogous Pt–CO counterparts, which is in consonance with its tendency to be released (Scheme 8).

Overall, the energy barriers of the pathway leading to cyclopropyl tricycle **4b** from **I1$_{et}$** are compatible with the thermal requirements of the reaction. The calculations suggest that the initial [4C + 3C] cycloaddition that delivers the carbene **I3$_{et}$** is the step with the highest energy barrier ($\Delta G^{\ddagger} = 8.9$ kcal mol^{-1}). After conformational evolution to **I3′$_{et}$**, a 8.2 kcal mol^{-1} energy barrier connects this carbene species with **I4′$_{et}$**, and eventually with the tricyclic product **4b**.

Key steps in the gold(ı)-catalyzed process. The energy profile for the allenediene **1b**, using [(C$_6$F$_5$)$_3$P–Au]$^+$ as a model catalyst, is shown in Fig. 6 (related to Table 1, entry 7). Interestingly, the
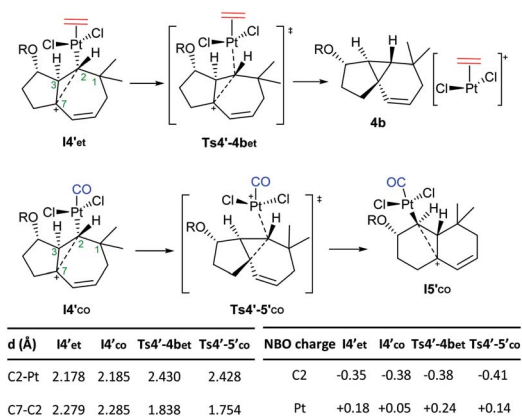
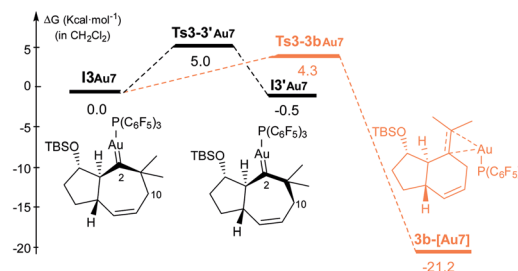**Scheme 8** Divergent paths observed with CO and ethene ligands from species **I4′**. Key distances and NBO charges.[22]

Fig. 6 Key steps of the Gibbs energy profile of the reaction of **1b** catalyzed by [(F$_5$C$_6$)$_3$P–Au]$^+$, in CH$_2$Cl$_2$.[22]

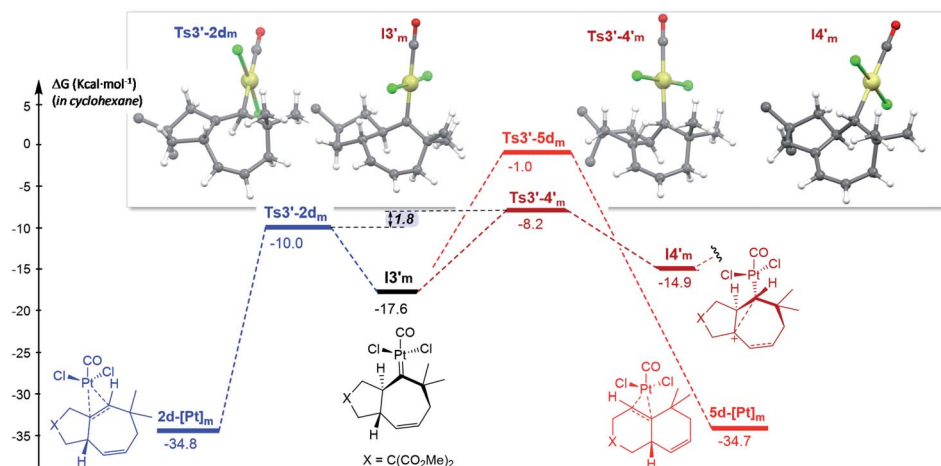**Fig. 7** Gibbs energy profile for the reaction of **1d** catalyzed by PtCl$_2$(CO) in cyclohexane; energy of **I1m** (Fig. S15†) is considered as the reference. The gem-diesters [X = C(CO$_2$Me)$_2$] are omitted for clarity. See Fig. S15 and S16† for the entire energy profile.[22]

ring contraction of the gold-carbene intermediate **I3$_{Au7}$** to give the experimentally observed cyclohexenyl adduct **3b**, is more easily achieved than in the case of the Pt catalysts [($\Delta G^{\ddagger}$ = 4.3 kcal mol^{-1} vs. 12.5 kcal mol^{-1} for PtCl$_2$(CO) and 15.6 for PtCl$_2$(ethene)]. The corresponding transition state, **Ts3-3b$_{Au7}$**, even sits energetically below that corresponding to the conformational change towards **I3′$_{Au7}$** (**Ts3-3′$_{Au7}$**). The ease of the ring contraction seems to be related to the carbocationic nature of the C2-carbene center, which favors the orbital interactions with C10. Therefore, our calculations are in qualitative agreement with the experimentally observed selectivity towards the [4 + 2] adduct **3b** using gold complexes bearing π–acceptor ligands (e.g. **Au7** or **Au3**).[34]

Influence of the connecting tether: reaction profile for 1d in the presence of PtCl$_2$(CO). Overall, the above calculations have provided a quite comprehensive mechanistic overview of the reactivity of allenedienes such as **1a** and **1b**. But, why does the analogous precursor **1d**, lacking the OTBS group, behave in such a different way? To shed light on this dichotomy we performed a computational analysis on the evolution of **1d**, using PtCl$_2$(CO) as the catalyst (Fig. 7, S15 and S16†).

The formation of carbene **I3$_m$** through a concerted [4C(4π) + 3C(2π)] cycloaddition proceeds with an energy barrier similar to that observed in previous cases, albeit now there are no significant conformational preferences within the ensuing five membered ring ($\Delta\Delta G^{\ddagger}$ = 0.3 kcal mol^{-1}, Fig. S15†).[35] Platinum carbene intermediate, **I3$_m$**, can also easily evolve to its conformer **I3′$_m$**, which is almost isoenergetic (Fig. S15†). Remarkably, in contrast to what was observed for **1b**, the most energetically favored evolution of **I3′$_m$** is the 1,2-hydrogen migration leading to the cycloheptene adduct **2d** (**Ts3′–2d$_m$**, $\Delta G^{\ddagger}$ = 7.6 kcal mol^{-1}, Fig. 7).[36] The alternative pathway observed for substrate **1b**, involving the 1,3-hydrogen migration and generation of carbocationic species **I4′$_m$** is almost 2 kcal mol^{-1} more costly (Fig. 7).

A stepwise pathway leading to the decalin **5d** from **I4′$_m$** could not be located, whereas the direct migration of C7, through **Ts3′-5d′$_m$** presents the highest energetic barrier (>16 kcal mol^{-1},

Fig. 7). Therefore, in consonance with the experimental results the most favored pathway is that leading to the [4C + 3C] adduct **2d**.

Comparing the energy profiles of **1d** and **1b** it can be seen that the barrier associated with the formation of cycloheptene **2d** (via **Ts3′-2d$_m$**) is 2.2 kcal mol^{-1} lower than that required for obtaining the analog [4C + 3C] adduct **2b** from **1b** (via **Ts3′-2b$_{co}$**, Fig. 8). Moreover, the highest energy barrier in the pathway towards products of type **5** and **4**, requiring first the migration of the hydrogen at C7 into the metal carbene center (C2), is considerably higher in the case of the substrate **1d** than with **1b** [$\Delta\Delta G^{\ddagger}$ = 3.4 kcal mol^{-1}, Fig. 8].[37] Therefore, for substrate **1b**, with the OTBS pendant in the connecting tether, there is destabilization of transition state **Ts3′-2b′$_{co}$** and stabilization of **Ts3′-4′$_{co}$**, and both effects synergistically contribute to the switch of selectivity compared to allenedienes such as **1d**.
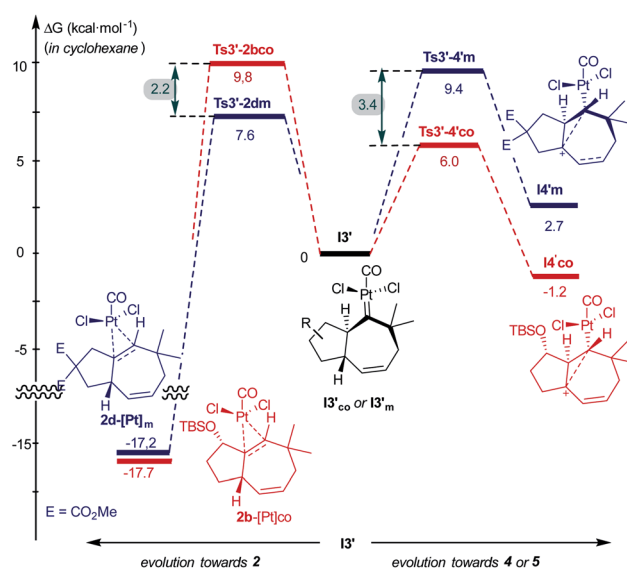

Fig. 8 Comparison of energy barriers in pathways to cycloheptene **2** and adducts **4/5**, from **1b** and **1d**; energies of **I3′$_{co}$** and **I3′$_m$** are used as the reference.
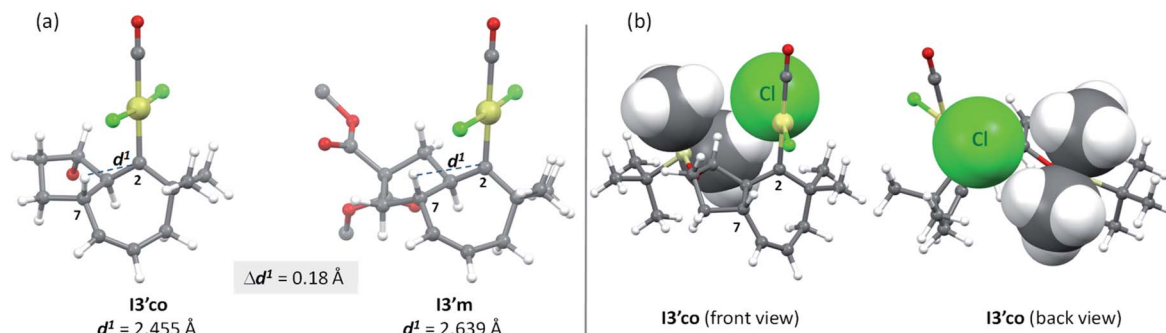
Fig. 9 Comparison of H7–C2 distances in I3′$_{co}$ and I3′$_m$ (a), and major steric repulsions within I3′$_{co}$ (b); space filling models using Van del Waals radii are used in specific atoms to highlight the steric interactions.

But, what are the physical reasons behind these differences? The stabilization of the transition state **Ts3′-4′$_{co}$**, corresponding to the migration of the hydrogen atom at C7 to the carbene center, can be qualitatively understood by analyzing the conformations of their immediate precursor **I3′$_{co}$**. In particular, the distance between the hydrogen atom that migrates from C7 to C2 is significantly shorter in **I3′$_{co}$** than in **I3′$_m$** [Fig. 9a, d(H7–C2) = 2.455 Å in **I3′$_{co}$** and 2.639 Å in **I3′$_m$**]. These differences are likely associated with a steric clash in **I3′$_{co}$**, between one of the methyl groups of the TBS moiety and the chloride atom at the platinum center. This steric congestion forces the Pt center to move far from the methyl, eventually resulting in a higher proximity of the H7 to the empty p-orbital of the carbene at C2 (Fig. 9b). As a result, the orbital contact for the 1,3-hydride migration towards **I4′$_{co}$** is facilitated, favoring the overall process towards **5** and **4**.

Moreover, the destabilization of the transition state leading to cycloheptene **2b** (**Ts3′-2b$_{co}$**) can be understood by considering stereoelectronic factors imposed by the OTBS group. During the required 1,2 H migration (from C3 to C2), the TBS group gets quite close to the [PtCl] moiety (Fig. 10a). Moreover, the positive charge generated at the ensuing sp^2 carbon, C3, is further intensified by inductive effects generated by the oxygen atom at its β position (see Fig. 10 for atomic charges). In this regard, NBO analysis of this transition state did not show any hyperconjugative interaction, between C3 and the oxygen lone pairs, which could stabilize this positive charge of C3.[38] In contrast, in the analog transition state from **1d** (**Ts3′-2d$_m$**, Fig. 10b), there are no such destabilizing interactions, while the positive charge generated at C3 is stabilized by hyperconjugation with its adjacent C4–H bond (NBO analysis, Fig. 10b).

Thus, all these stereoelectronic factors synergistically contribute to determination of the fate of the cycloheptene carbene intermediates.

Importantly, while these results arise from the analysis of specific substrates, the mechanistic findings are relevant to other reactions that occur through similar types of intermediates.

Conclusions

To conclude, the presence of a bulky silyl ether substituent in the connecting tether of allenedienes of type **1**, allowed the exploration of novel, intramolecular annulations promoted by carbophilic catalysts. Remarkably, the different pathways can be finely tuned by choosing appropriate ligands at the metal center, which helped to obtain a variety of carbocyclic skeletons in a divergent and highly stereoselective manner.

The unexpected rearrangements revealed a number of previously unidentified, mechanistic features that are related to the whole field of synthetic and organometallic chemistry. The effect of a CO ligand in the evolution of platinum intermediates formed after the initial [4C + 3C] cycloaddition step is specifically significant. The presence of the CO ligand hampers the release of the platinum complex from key intermediates, and favors rearrangement processes involving non-classical cationic intermediates which are stabilized by homo-hyperconjugation. These types of interactions, almost ignored in Pt catalysis, should be taken into account when designing other skeletal rearrangements. Finally, we also demonstrate how the obtained annulation products can be
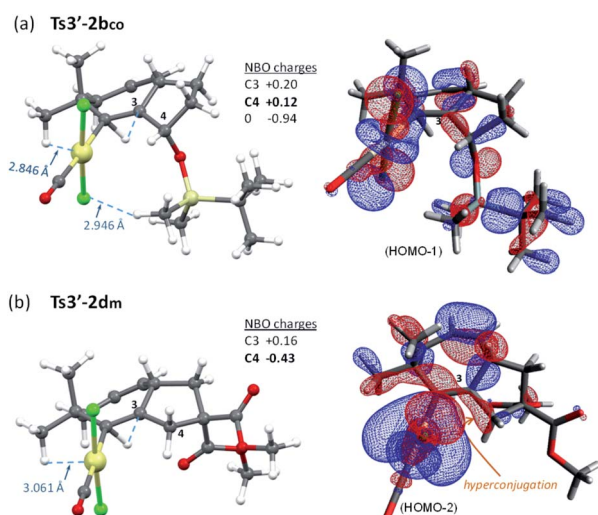

Fig. 10 Comparison of steric repulsions (a) and the most relevant HOMO orbitals (b) of **Ts3′-2b$_{co}$** and **Ts3′-2d$_m$** (NBO analysis).

selectively manipulated, paving the way for the synthetic applications of this methodology.

Conflicts of interest

There are no conflicts to declare.

Acknowledgements

Notes and references

1 (*a*) A. S. K. Hashmi and G. J. Hutchings, *Angew. Chem., Int. Ed.*, 2006, **45**, 7896–7936; (*b*) D. J. Gorin and F. D. Toste, *Nature*, 2007, **446**, 395–403; (*c*) A. Fürstner, *Acc. Chem. Res.*, 2014, **47**, 925–938; (*d*) R. Dorel and A. M. Echavarren, *Chem. Rev.*, 2015, **115**, 9028–9072; (*e*) D. Pflästerer and A. S. K. Hashmi, *Chem. Soc. Rev.*, 2016, **45**, 1331–1367; (*f*) Z. Zheng, Z. Wang, Y. Wang and L. Zhang, *Chem. Soc. Rev.*, 2016, **45**, 4448–4458.

2 (*a*) J. L. Mascareñas, I. Varela and F. López, *Acc. Chem. Res.*, 2019, **52**, 465–479; (*b*) F. López and J. L. Mascareñas, *Beilstein J. Org. Chem.*, 2013, **9**, 2250–2264. see also: (*c*) D. C. Marcote, I. Varela, J. Fernández-Casado, J. L. Mascareñas and F. López, *J. Am. Chem. Soc.*, 2018, **140**, 16821–16833.

3 For the first Pt-catalyzed reaction of allenes, see: (*a*) C. Stephan, C. Munz and H. Tom Dieck, *J. Organomet. Chem.*, 1994, **468**, 273–278; see also: (*b*) T. Ishiyama, T. Kitano and N. Miyaura, *Tetrahedron Lett.*, 1998, **39**, 2357–2360; (*c*) Y. Yasunori, F. Ryou, Y. Akihiko and M. Norio, *Chem. Lett.*, 1999, **28**, 1069–1070; For the first Au-catalyzed reactions of allenes, see: (*d*) A. S. K. Hashmi, L. Schwarz, J.-H. Choi and T. M. Frost, *Angew. Chem., Int. Ed.*, 2000, **39**, 2285–2288; (*e*) A. S. K. Hashmi, T. M. Frost and J. W. Bats, *J. Am. Chem. Soc.*, 2000, **122**, 11553–11554; (*f*) A. Hoffmann-Röder and N. Krause, *Org. Lett.*, 2001, **3**, 2537–2538; (*g*) N. Krause, A. Hoffmann-Röder and J. Canisius, *Synthesis*, 2002, **2002**, 1759–1774.

4 (*a*) B. Trillo, F. López, S. Montserrat, G. Ujaque, L. Castedo, A. Lledós and J. L. Mascareñas, *Chem. – Eur. J.*, 2009, **15**, 3336–3339; (*b*) I. Alonso, B. Trillo, F. López, S. Montserrat, G. Ujaque, L. Castedo, A. Lledós and J. L. Mascareñas, *J. Am. Chem. Soc.*, 2009, **131**, 13020–13030; see also: (*c*)

I. Alonso, H. Faustino, F. López and J. L. Mascareñas, *Angew. Chem., Int. Ed.*, 2011, **50**, 11496–11500.

5 P. Mauleón, R. M. Zeldin, A. Z. González and F. D. Toste, *J. Am. Chem. Soc.*, 2009, **131**, 6348–6349.

6 For an interesting gold-catalyzed cycloaddition of alkyne-1,3-dienes, see: A. Fürstner and C. C. Stimson, *Angew. Chem., Int. Ed.*, 2007, **46**, 8845–8849.

7 (*a*) D. Benitez, E. Tkatchouk, A. Z. Gonzalez, W. A. Goddard and F. Dean Toste, *Org. Lett.*, 2009, **11**, 4798–4801; (*b*) S. Montserrat, I. Alonso, F. López, J. L. Mascareñas, A. Lledós and G. Ujaque, *Dalton Trans.*, 2011, **40**, 110095–111105; (*c*) A. H. Christian, Z. L. Niemeyer, M. S. Sigman and F. D. Toste, *ACS Catal.*, 2017, **7**, 3973–3978; For studies describing particular characteristics of gold-carbenes, see: (*d*) L. Nunes dos Santos Comprido, J. E. M. N. Klein, G. Knizia, J. Kästner and A. S. K. Hashmi, *Angew. Chem., Int. Ed.*, 2015, **54**, 10336–10340; (*e*) L. Nunes dos Santos Comprido, J. E. M. N. Klein, G. Knizia, J. Kästner and A. S. K. Hashmi, *Chem. – Eur. J.*, 2016, **22**, 2892–2895.

8 B. Trillo, F. López, M. Gulías, L. Castedo and J. L. Mascareñas, *Angew. Chem., Int. Ed.*, 2008, **47**, 951–954.

9 For other reports comparing Au and Pt catalytic profiles, see: (*a*) M. Pernpointner and A. S. K. Hashmi, *J. Chem. Theory Comput.*, 2009, **5**, 2717–2725; (*b*) A. Leyva-Pérez and A. Corma, *Angew. Chem., Int. Ed.*, 2012, **51**, 614–635; (*c*) A. S. K. Hashmi, E. Kurpejovic, W. Frey and J. W. Bats, *Tetrahedron*, 2007, **63**, 5879–5885.

10 R. Nelson, M. Gulías, J. L. Mascareñas and F. López, *Angew. Chem., Int. Ed.*, 2016, **55**, 14359–14363.

11 (*a*) M. Alcarazo, T. Stork, A. Anoop, W. Thiel and A. Fürstner, *Angew. Chem., Int. Ed.*, 2010, **49**, 2542–2546; see also: (*b*) B. W. Gung, D. T. Craft, L. N. Bailey and K. Kirschbaum, *Chem. – Eur. J.*, 2010, **16**, 639–644.

12 See for instance: G. Liu and D. Romo, *Angew. Chem., Int. Ed.*, 2011, **50**, 7537–7540.

13 See the ESI† for further details.

14 See for instance: M. I. Velazco, L. Wuensche and P. Deladoey, *Use of Cubebol as a Flavoring Ingredient*, EP1040765, Firmenich, S.A., 2000.

15 (*a*) A. Fürstner and P. Hannen, *Chem. – Eur. J.*, 2006, **12**, 3006–3019; (*b*) C. Fehr and J. Galindo, *Angew. Chem., Int. Ed.*, 2006, **45**, 2901–2904; (*c*) D. M. Hodgson, S. Salik and D. J. Fox, *J. Org. Chem.*, 2010, **75**, 2157–2168; (*d*) S. M. Kim, J. H. Park, S. Y. Choi and Y. K. Chung, *Angew. Chem., Int. Ed.*, 2007, **46**, 6172–6175; (*e*) C. Fehr, I. Magpantay, J. Arpagaus, X. Marquet and M. Vuagnoux, *Angew. Chem., Int. Ed.*, 2009, **48**, 7221–7223.

16 Allenedienes of type **1** can be synthesized in an asymmetric fashion using a Ru-catalyzed asymmetric transfer hydrogenation (see ref. 10), which paves the way for an enantioselective entry to these scaffolds.

17 C. M. Cerda-García-Rojas, A. D. C. Coronel, M. E. P. De Lampasona, C. A. N. Catalán and P. Joseph-Nathan, *J. Nat. Prod.*, 2005, **68**, 659–665.

18 The precedents on the effect of CO in the catalytic activity of PtCl₂ basically deal with changes in reaction rates and/or yields, see: (*a*) A. Fürstner, P. W. Davies and T. Gress, *J.*

Am. Chem. Soc., 2005, **127**, 8244–8245; (*b*) Y. Gimbert, L. Fensterbank, V. Gandon, J. P. Goddard and D. Lesage, *Organometallics*, 2013, **32**, 374–376; for an isolated example wherein the use of CO modifies the *endo vs. exo* selectivity of a cycloisomerization, see: (*c*) A. Fuente-Hernández, P. Costes, P. Kalck, U. Jáuregui-Haza, O. Dechy-Cabaret and M. Urrutigoïty, *Appl. Organomet. Chem.*, 2011, **25**, 815–819.

19 The structure of **6b** could be determined by X-ray analysis of a derivative. See the ESI† for details.

20 Although the oxidative trapping of monosubstituted Pt- and Au-carbenes is known, that of disubstituted carbenes is almost unprecedented, due to their lower reactivity; see reference **4a** and: S. Montserrat, H. Faustino, A. Lledòs, J. L. Mascareñas, F. López and G. Ujaque, *Chem. – Eur. J.*, 2013, **19**, 15248–15260.

21 Very few, isolated examples of C–H insertions with concomitant cyclopropanation have been reported with Pt or Au-carbene species. For **Au**, see: (*a*) Y. Horino, T. Yamamoto, K. Ueda, S. Kuroda and F. D. Toste, *J. Am. Chem. Soc.*, 2009, **131**, 2809–2811; (*b*) G. Lemière, V. Gandon, K. Cariou, A. Hours, T. Fukuyama, A. L. Dhimane, L. Fensterbank and M. Malacria, *J. Am. Chem. Soc.*, 2009, **131**, 2993–3006; (*c*) A. Escribano-Cuesta, V. López-Carrillo, D. Janssen and A. M. Echavarren, *Chem. – Eur. J.*, 2009, **15**, 5646–5650. For **Pt**, see: (*d*) H. Funami, H. Kusama and N. Iwasawa, *Angew. Chem., Int. Ed.*, 2007, **46**, 909–911; (*e*) C. H. Oh, J. H. Lee, S. M. Lee, H. J. Yi and C. S. Hong, *Chem. – Eur. J.*, 2009, **15**, 71–74.

22 (*a*) DFT calculations have been carried out with Gaussian 09. The geometries of all species were optimized using the B3LYP hybrid functional together with the 6-31G(d) basis set for C, H, O, P, Si and Cl and the LANL2DZ basis set for Pt and Au. Single-point calculations of the optimized systems were carried out using hybrid functional M06 together with the 6-3111++g(d,p) basis set for C, H, O, P, Si and Cl, and the Stuttgart-Dresden (SDD) ECP for Pt and Au, either in cyclohexane (for Pt catalysis) or dichloromethane (for gold catalysis) as solvents (using the SMD model). See the ESI† for further details and references; (*b*) For clarity reasons, we depicted the enantiomeric series.

23 According to previous reports, we considered $PtCl_2(CO)$ as the active catalyst generated from $PtCl_2$/CO; see ref. 18b and (*a*) H. Alper, Y. J. Huang, D. B. Dellamico, F. Calderazzo, N. Pasqualetti and C. A. Veracini, *Organometallics*, 1991, **10**, 1665–1671; (*b*) D. B. Dell'Amico, R. Bini, F. Calderazzo, L. Carbonaro, L. Labella and A. Vitullo, *Organometallics*, 2005, **24**, 4427–4431; (*c*) D. B. Dell'Amico, R. Bini, F. Calderazzo, L. Carbonaro, L. Labella and A. Vitullo, *Organometallics*, 2006, **25**, 4913–4916; Moreover, according to the literature, the reduction of Pt(II) to Pt(0) under these conditions seems very unlikely, see: (*d*) D. A. Evans, M. F. Hallam, D. M. P. Mingos and R. W. Wardle, *J.*

Chem. Soc., Dalton Trans., 1987, 1889–1895; (*e*) See also the ESI for control experiments with Pt(0) complexes.

24 A complete computational analysis from the pseudo-equatorial conformer ($I3_{co}^{eq}$) was also carried out but we could not locate more favored pathways towards any of the products. Indeed, the lowest energy pathway involves a transition state in which the OTBS group is relocated in a *pseudo*-axial disposition (Fig. S9†).

25 (*a*) I. V. Alabugin, G. dos Passos Gomes and M. A. Abdo, *Wiley Interdiscip. Rev.: Comput. Mol. Sci.*, 2019, **9**, e1389; (*b*) Z. Alamiddine and S. Humbel, *Front. Chem.*, 2014, **1**, 1–9.

26 (*a*) NBO calculations did not provide any HOMO or HOMO-*n* molecular orbital featuring an allyl cation bonding interaction between C7, C8 and C9; (*b*) The orbital HOMO−1 is considered instead of the HOMO since the latter exclusively involves the $[PtCl_2]$ moiety. The energy difference between them is 0.34 eV.

27 Related non-classical Pt-stabilized carbocationic intermediates were only proposed by Gagné in the context of cycloisomerization of 1,6-dienes, see: F. Bell, J. Holland, J. C. Green and M. R. Gagné, *Organometallics*, 2009, **28**, 2038–2045.

28 From intermediate $I3'_{co}$, we could not locate a 1,2-alkyl (C10) migration leading to the formal [4 + 2] adduct **3b**, likely due to an unfavorable conformation.

29 (*a*) M. Brookhart and Y. Liu, *J. Am. Chem. Soc.*, 1991, **113**, 939–944; (*b*) C. P. Casey and N. A. Strotman, *J. Am. Chem. Soc.*, 2004, **126**, 1699–1704; (*c*) J. B. Lambert, L. A. Salvador and J. H. So, *Organometallics*, 1993, **12**, 697–703.

30 We also located an analogous route towards **5b** from the initial conformer $I3_{co}$, through related species $I4_{co}$ and $I5_{co}$ (Fig. S8B†). Nonetheless, this route is significantly less favored than that from $I3'_{co}$.

31 Additionally, we theoretically analyzed the reaction of 1b with the catalyst resulting from $PtCl_2/P(C_6F_5)_3$ (Table 1, entry 13). The energy profile (Fig. S13†) is not significantly different from that found for $PtCl_2$(ethene).

32 For an isolated case with a Pt-vinylidene, see: (*a*) Z. F. Li, Y. Fan, N. J. Deyonker, X. Zhang, C. Y. Su, H. Xu, X. Xu and C. Zhao, *J. Org. Chem.*, 2012, **77**, 6076–6083; In general, stepwise $C(sp^3)$–H insertions on metal carbenes are rare. A handful of feasible cases involving Rh and Au carbenes have been proposed when stable carbocations are generated from the initial hydride migration, see: (*b*) J. Hansen, J. Autschbach and H. M. L. Davies, *J. Org. Chem.*, 2009, **74**, 6555–6563; (*c*) S. Bhunia and R.-S. Liu, *J. Am. Chem. Soc.*, 2008, **130**, 16488–16489; (*d*) Y. Wang, Z. Zheng and L. Zhang, *J. Am. Chem. Soc.*, 2015, **137**, 5316–5319.

33 This trend is observed in all stationary points throughout the energy profiles with $PtCl_2$(CO) and $PtCl_2$(ethene).

34 For a related preliminary analysis with a $[IPrAu]^+$ model catalyst related to **Au1**, also consonant with the experimental results, see Fig. S14.†

35 Both conformations of the ensuing five-membered ring were analyzed and the energy difference between them was

negligible (see Fig. S15†). Nonetheless, the most favored one, analogous to the previously denoted as *pseudo*-equatorial, has been considered for Fig. 7 (see the full profile in Fig. S16†).

36 Moreover, the next favoured process is the homologous 1,2-H migration from the conformer $I3_m$ (*via* $Ts3$-$2d_m$, $\Delta G^{\ddagger} = 8.1$ kcal·mol^{-1}, Fig. S16†).

37 Similar trends are also observed when analyzing the homologous pathways from the conformers $I3_m$ and $I3_{co}$ (Fig. S17†).

38 J. S. Kudavalli and R. A. More O'Ferrall, *Beilstein J. Org. Chem.*, 2010, **6**, 1035–1042.